

Nanoscale

Accepted Manuscript



This is an *Accepted Manuscript*, which has been through the Royal Society of Chemistry peer review process and has been accepted for publication.

Accepted Manuscripts are published online shortly after acceptance, before technical editing, formatting and proof reading. Using this free service, authors can make their results available to the community, in citable form, before we publish the edited article. We will replace this *Accepted Manuscript* with the edited and formatted *Advance Article* as soon as it is available.

You can find more information about *Accepted Manuscripts* in the [Information for Authors](#).

Please note that technical editing may introduce minor changes to the text and/or graphics, which may alter content. The journal's standard [Terms & Conditions](#) and the [Ethical guidelines](#) still apply. In no event shall the Royal Society of Chemistry be held responsible for any errors or omissions in this *Accepted Manuscript* or any consequences arising from the use of any information it contains.

High-speed detection of DNA Translocation in Nanopipettes

*Raquel L. Fraccari¹, Pietro Ciccarella², Azadeh Bahrami¹, Marco Carminati², Giorgio Ferrari²,
Tim Albrecht^{1*}*

¹ Imperial College London, Department of Chemistry, Exhibition Road, London SW7 2AZ, UK

² Politecnico di Milano, Dipartimento di Elettronica, Informazione e Bioingegneria, P.za
Leonardo da Vinci 32, Milano, Italy

We present a high-speed electrical detection scheme based on a custom-designed CMOS amplifier which allows the analysis of DNA translocation in glass nanopipettes on a microsecond timescale. Translocation of different DNA lengths in KCl electrolyte provides a scaling factor of the DNA translocation time equal to $p = 1.22$, which is different from values observed previously with nanopipettes in LiCl electrolyte or with nanopores. Based on a theoretical model involving electrophoresis, hydrodynamics and surface friction, we show that the experimentally observed range of p -values may be the result of, or at least be affected by DNA adsorption and friction between the DNA and the substrate surface.

Keywords: scaling factor, DNA, bandwidth, nanopipettes, nanopores

Nanopipettes have emerged as a new class of solid-state nanopore sensors, which allow for the detection of DNA, proteins and DNA/protein complexes.¹⁻³ In comparison with "classical", chip-based nanopore sensors they are less amenable to mass fabrication and it is difficult to routinely achieve very small pores with diameters below 10 nm.⁴ However, they also exhibit a range of advantages, including ease of fabrication, robustness, excellent wettability with aqueous electrolytes and facile integration into microfluidic systems.^{2,3,5-8} Entirely made out of glass, nanopipettes exhibit very low device capacitance and dissipation factors (< 10 pF and $D \approx 0.02$, see below) and therefore in principle superior noise performance, compared to conventional Si-based nanopore chips, and similar to the ultra-low noise performance of quartz- and pyrex-based nanopore devices.^{3,8-11}

Compared to chip-based nanopore devices, there are also more subtle differences, for example with regards to the electric field distribution around the pore opening. In the former case, the electric field drops relatively rapidly and symmetrically on both sides of the pore. DNA capture occurs in an approximately hemispherical volume around the pore entrance, outside of which Brownian motion is dominant.¹² In the case of a sharp nanopipette, the capture volume on the outside of the pipette is large, while inside the pipette it is confined by the glass walls. The local electric field decays quickly on the outside, but relatively slowly on the inside of the pipette (for a given solution resistivity). Accordingly, the translocation frequency, the dynamics of the polymer during translocation and perhaps the mechanism of translocation may be affected, and potentially depend on the direction of transport. This would in turn be reflected in characteristic parameters of the translocation process, such as the translocation time, its distribution and DNA length dependence of the translocation time.

It is thus interesting to note that the scaling factor p of the translocation time τ for (double-stranded) DNA vs. the polymer length L_{DNA} , i.e. $\tau \propto (L_{\text{DNA}})^p$, was indeed found to vary. In some cases, mainly for chip-based nanopores with Si_3N_4 or SiO_2 membranes in KCl electrolyte, p was found to be ≈ 1.3 .^{13–18} In particular, Storm *et al.* found a scaling factor of 1.27 experimentally for L_{DNA} between 6.6 and 97 kbp.¹⁴ This compared well with their theoretical estimate of 1.22, based on the interplay between hydrodynamic forces on the DNA 'blob' at the pore entrance and electrophoretic drag on the DNA inside the pore. On the other hand, Bell *et al.* found $p \approx 1$ for the translocation of DNA through nanopipettes in LiCl electrolyte (in fact, p slightly smaller than 1 for $L_{\text{DNA}} < 4$ kbp and slightly larger than 1 for $L_{\text{DNA}} > 4$ kbp).¹⁹ This is in accordance with a translocation model, as proposed by Ghosal, which also takes into account the structure of the electric double layer and hydrodynamic drag inside the channel.^{20,21}

This raises the question as to whether the observed values for p actually reflect properties of the polymer, of the solution environment (which may in turn affect the polymer) or rather other features of the translocation process. Accordingly, Bell *et al.* hypothesized that DNA adsorption could lead to $p > 1$, however without providing a detailed quantitative explanation.¹⁹ Following their argument, when translocating DNA from the outside to the inside of a nanopipette, the high aspect ratio of the latter would render DNA adsorption prior to translocation unlikely and hence $p \approx 1$. The importance of DNA/surface interactions during translocation in very small Si_3N_4 pores (diameters < 10 nm) has been studied in detail by Wanunu and Meller.¹⁷ Apart from very fast, "collision" events, they observed two populations of DNA translocation events, characterized by translocation times t_1 and t_2 ($t_1 < t_2$), where population 1 was dominant for short and population 2 dominant for long DNA. Both t_1 and t_2 were found to depend on DNA length,

namely with scaling factors of $p_1 = 1.40 \pm 0.05$ and $p_2 = 2.28 \pm 0.05$, and decreased exponentially with increasing bias voltage V_{bias} . Moreover, a reduction in pore diameter lead to an increase in the translocation time that was thought to be incommensurate with the increased viscous drag inside the pore. Finally, a decrease in temperature from 30 to 0 °C lead to an increase in the translocation time that was too large for it to be based on viscosity increase alone. Taken together, these arguments suggested that DNA/surface interactions are an important factor governing the translocation process. They also argue that the occurrence of the longer time scale t_2 may be related to interactions between the DNA outside the pore (where the electric field is relatively weak) and the membrane. This is reminiscent of Bell's argument above and the observation of the increased scaling factor lends further support to this idea. However, again no quantitative model was developed to assess the effect of DNA adsorption outside the pore channel on the scaling behavior.

Here, we set out to shed light into this fundamentally important question and study, for the first time, the length dependence of (double-stranded) DNA translocation in nanopipettes in KCl electrolyte, i.e. in solution conditions similar to most nanopore-based experiments. Translocation of DNA in KCl is typically much faster than in other alkali halides.²² We therefore employed custom-designed electronics allowing for low-current, wide-bandwidth detection of translocation events in nanopipettes,²³ and studied four different DNA lengths ($L_{\text{DNA}} = 4; 5.31; 10$ and 48.5 kbp, see figure S1 in the SI for gel electrophoresis data) at bias voltages V_{bias} ranging from -200 to -900 mV. We find an average scaling factor $p = 1.22 \pm 0.01$, independent of V_{bias} . To explore whether surface effects could explain the variation in observed scaling factors, we extended Ghosal's model, to include a friction term that describes the DNA sliding over the solid surface while being pulled into the pore by the electric field. As we show below, this extended model

indeed predicts $1 \leq p \leq 2$, depending on the level of friction and DNA length. Interestingly, for low to intermediate values of the friction coefficient β , as determined from AFM pulling experiments with (bio)polymers on mica,²⁴ p is similar to what is observed for chip-based nanopores. While the numerical agreement may be fortuitous, given the simplicity of the model, those findings reinforce the potential importance of DNA adsorption outside the pore with regards to DNA translocation time and the translocation process as a whole.

We start the discussion with the custom-designed electronics. A schematic of the setup is shown in Figure 1 (for further details, also a comparison with previously reported setups, see section 2 in the SI). The electronic circuit is based on a low-noise, wide-bandwidth CMOS current amplifier, which drastically reduces the parasitic input capacitance and thus strongly improves the noise performance. The low-noise amplifier is based on an integrated current amplifier designed in 0.35 μm CMOS technology. The integration in a single chip of the input stages of the amplifier has reduced the input capacitance to ≈ 2 pF with a beneficial effect on the high frequency noise. A current amplification without noisy resistors is obtained using matched transistors and capacitors, as described by Ferrari et al.²⁵ Briefly, the input current is converted into a voltage by the feedback devices (M_{p1} , C_1 , M_{n1}) and then reconverted into current by M_{p2} , C_2 , M_{n2} obtaining a wide-band current amplification given by the geometric ratio between the output devices and the feedback devices, 99 in our case. The second stage based on OP2 gives a further current amplification of ten based on the same principle. The amplified current is converted into a voltage by the off-chip transimpedance amplifier (TIA). Current pre-amplification breaks the noise/bandwidth trade-off of conventional transimpedance amplifiers, based on feedback resistor. Indeed, in the absence of the CMOS amplifier, the feedback resistor

of the TIA, R_5 , would have set the noise performance, total gain and bandwidth limited by its parasitic parallel capacitance C_5 . The high gain of the current amplifier (990) reduces the effect of the thermal noise of $R_5 = 51 \text{ k}\Omega$ to a negligible value (equivalent input noise of $0.6 \text{ fA}/\sqrt{\text{Hz}}$) maintaining a bandwidth of the amplifier greater than 1 MHz (Fig. S3). The large DC current coming from the nanopipette (up to $\pm 100 \text{ nA}$) flows in the resistor R_1 thanks to a suitable feedback network operating at low frequency (less than 10 Hz).²³ Thus, the fast path provided by the current amplifier and the TIA amplifies the short pulses given by the pore blockade irrespective of the DC current and low-frequency fluctuations of the ionic current. The value of the bias current is obtained by measuring the voltage drop on the resistor R_1 . In addition, the AC coupling of the CMOS current amplifier provided by the DC feedback network minimizes the shot noise of the M1-M4 transistors operating in sub-threshold regime. The low-noise amplifier is placed inside the Faraday cage as close as possible to the nanopipette to minimize the parasitic capacitance of connecting wires and the coupling of interferences. Detailed noise characterization reveals that above 100 kHz the setup is comparable to the most powerful systems that are currently available, achieving an input rms current noise of 50 pA at 1 MHz bandwidth (open circuit condition, input capacitance of the amplifier and connector of $\approx 5 \text{ pF}$, see section 2 in the Supporting Information).^{26,27}

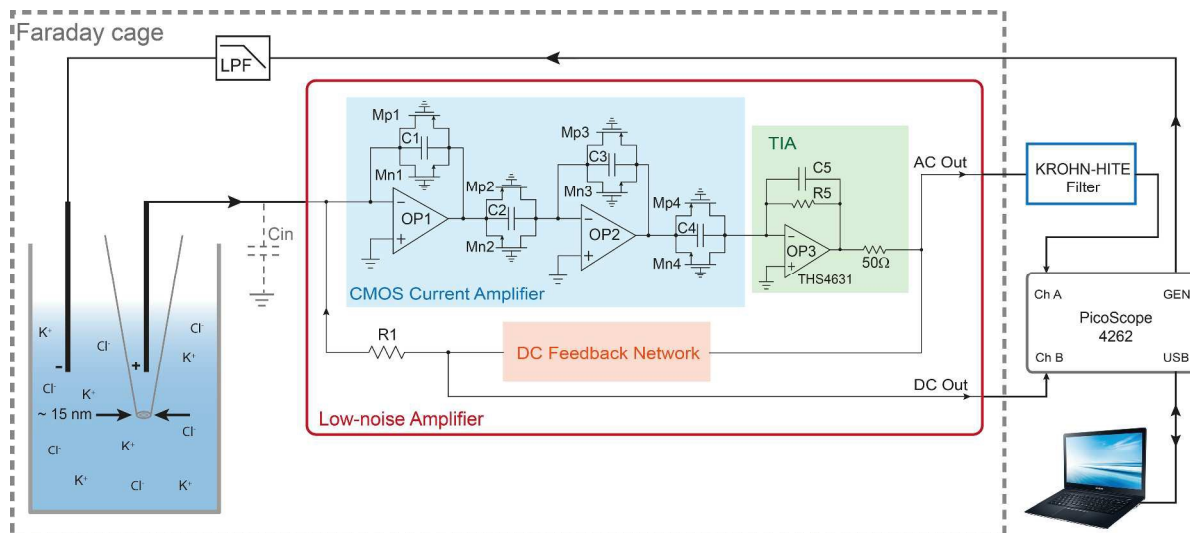


Figure 1. Low-noise measurement setup optimally coupling a low-capacitance glass nanopipette with a custom-designed CMOS amplifier that is the core of the dedicated and compact instrument providing up to 3 MHz bandwidth.

To test this new design, we performed DNA translocation experiments with nanopipettes in KCl electrolyte, in which DNA is known to translocate much faster than in LiCl or NaCl (see above). This has proven a challenging scenario for such experiments in nanopipettes.

However, the custom-built electronics have allowed filtering (of the AC channel) at up to 200 kHz bandwidth (8th order Bessel low pass filter) at $S/N > 10$ and DC input currents of up to 100 nA. Nanopipettes were made from plasma cleaned quartz capillaries that were pulled on a laser pipette puller (P200, Sutter Instruments, Novato, USA). Two freshly prepared Ag/AgCl electrodes were used for each experiment, one placed inside each of the electrolyte-filled compartments. The amplifier was connected to the electrode placed inside the nanopipette. The smaller size of this environment with respect to the external compartment reduces the stray capacitance and the electromagnetic interferences. Prior to use the pore conductance of each nanopipette was measured by performing an $I-V_{\text{bias}}$ curve. The nanopipettes used for these experiments had an Ohmic response in 1 M KCl and based on their conductance, the diameters

were estimated to be between 10 - 22 nm (14 nanopipettes in total), cf. section 3 in the SI.¹⁰ For each experiment, DNA was added to the external compartment ($c_{\text{DNA}} = 100 - 300 \text{ pM}$) and upon applying V_{bias} to the electrode outside the nanopipette, the negatively charged DNA translocated from outside to inside the nanopipette.

We studied translocation of four different DNA samples with lengths $L_{\text{DNA}} = 4; 5.31; 10$ and 48.5 kbp in a bias range from -200 to -900 mV . For each sample, several repeat translocation experiments were performed, using a different nanopipette for each (cf. Figure S7). Figure 2a shows a typical $I(t)$ trace recorded in the presence of 5.31 kbp dsDNA, with a few examples of individual events in panel b. The ionic current was filtered at 100 kHz (8^{th} order Bessel filter) giving a time resolution on the order of $7.0 \mu\text{s}$. The individual spikes in the $I(t)$ trace only occur in the presence of DNA and are temporal reductions in the current with a magnitude ΔI and a duration τ , as expected under high ionic strength conditions.²⁸ A scatter plot ΔI vs. τ with over 500 events is shown in Figure 2c with the corresponding τ and ΔI histograms displayed alongside the axes.

Apart from very short events, which we assign to either residual noise or 'collision' events (vide supra), we generally found two populations in the data. The population at longer τ and smaller ΔI to the translocation of linear DNA (red, group 1), while the population at shorter τ and higher ΔI encompasses translocation of folded DNA (blue, group 2).^{3,31} This is supported by an analysis of the signal shape, fig. 2b. In the following, the analysis of the length dependence focuses on the well-defined, linear events. To this end, a two-component Gaussian Mixture Model (GMM) was employed to improve the separation between the populations, which were then fitted with a suitable probability density function (PDF), see SI section 4 for further details.

We found the translocation time distributions to be somewhat asymmetric and well represented by log-normal distributions. We also attempted to fit the results using the probability density function (PDF) derived by Ling and Ling, based on a Schrödinger first-passage model, SI section 6.^{29,30} In principle, the latter would be preferable, due to the direct link to the physical basis of the process and the ability to extract physically relevant parameters, such as the diffusion coefficient and the translocation speed. However, we found the fit represented the translocation time distribution less accurately, and given our focus on the most probable translocation time τ_{mp} , we used the (rather more empirical) log-normal distribution instead.

Based on four nanopipettes, for the linear population the average τ_{mp} obtained is 0.137 ± 0.009 ms and the most probable $\Delta I = 82 \pm 3$ pA. The results for the other DNA lengths studied are shown in figure 3 below (for $V_{bias} = -0.8V$) and in the SI.

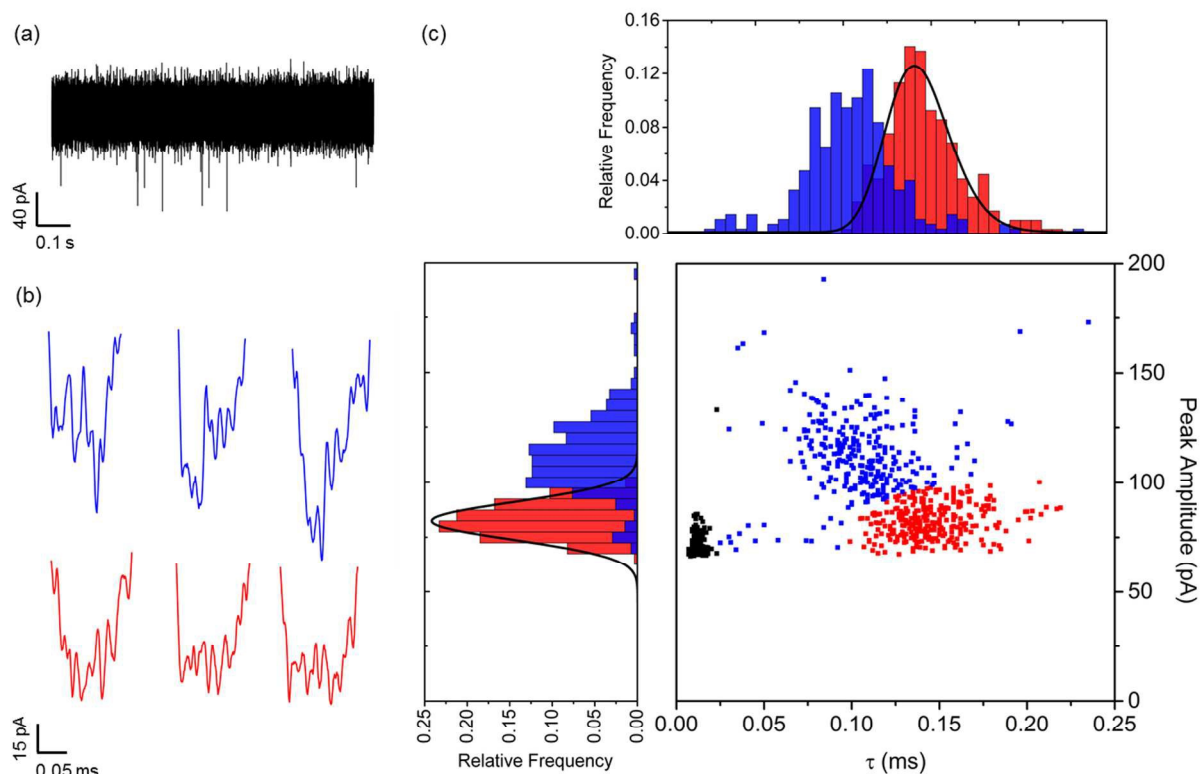


Figure 2. Translocation data for 5.31 kbp dsDNA with V_{bias} of -400 mV (filter frequency: 100 kHz). (a) Typical current versus time trace in the presence of 5.31 kbp dsDNA in the external compartment (cDNA = 300 pM). (b) Examples of folded translocation events with a large peak amplitude (top panel) and linear translocation events with a small peak amplitude (bottom panel). (c) Scatter plot of ΔI vs. τ with the corresponding peak amplitude and dwell time histograms. Linear translocation events are shown in red while folded translocation events are shown in blue. Events shown in black were attributed to noise and excluded from the peak selection. The peak amplitude distribution of the linear population is fitted with a Gaussian distribution, the corresponding dwell time distribution with a log-normal distribution.

The data was analyzed as described above (cf. SI for a full set of results). In all cases, we were able to fit the translocation time distribution for group 1 with a single, log-normal distribution.

Finally, we investigated the length dependence of τ for group 1, for a wide range of V_{bias} values. For a given L_{DNA} , we found τ_{mp} to be linearly dependent on V_{bias}^{-1} , with slopes m of 0.715 ± 0.116 , 0.112 ± 0.009 , 0.062 ± 0.003 , 0.037 ± 0.003 ms·V for 48.5, 10, 5.31 and 4 kbp DNA, figure 4a. This is in line with the Ghosal model and previous experimental results with chip-based nanopores,^{32,33} but different to reference 17 where an exponential dependence was observed. Moreover, we found m to be linearly dependent on L_{DNA} and determined the slope to be 0.0153 ± 0.0003 ms·V/kbp (intercept = -0.027 ± 0.008 ms·V, $R = 0.999$).

Figure 4b shows a double logarithmic plot of τ_{mp} vs. L_{DNA} for each V_{bias} as well as linear fits. As discussed above, the slope of these fits corresponds to the scaling factor p , which we found to be independent of V_{bias} and equal to 1.22 ± 0.01 (averaged over all V_{bias} , values between 1.17 and 1.26, cf. Table S3 in the SI). This is significantly higher than the result by Bell et al. for DNA translocation in nanopipettes in LiCl and the prediction by the Ghosal model ($p = 1$). It is very close to the theoretical prediction in reference 14, but still lower than many experimental values obtained with chip-based nanopores (1.27 and higher).^{14,17}

Given the limited size of our data set, we wondered about the statistical power of the scaling factor obtained above. Indeed, the extraction of scaling parameters and their statistical significance from log-log representations is known to be problematic, as discussed by Clauset et al.³⁴ They suggest a rigorous approach to extracting those parameters, which is however limited to $p > 1$. In the present case, we would like to specifically include the case of $p = 1$, and hence we decided to use stochastic simulations as a different approach. Details including the MATLAB simulation script are

given in the SI, section 7. Briefly, as an example we took the experimental mean τ_{mp} values and their standard deviations (based on three independent measurements) for each DNA length at a given bias (-400 mV). For this data set, we obtained $p = 1.235 \pm 0.052$ (the error is larger, compared to the "all dataset" value of ± 0.01 , due to the smaller number of observations). We scaled the mean values by $1/p$, such that the actual scaling law was modified to $p = 1$. The standard deviations were not scaled, which correspond to allowing for a larger error for each set of τ_{mp} values (more conservative estimate). We then 1) generated three Gaussian-distributed random numbers for each L_{DNA} (as in the experiment), 2) plotted their respective averages in a log-log representation vs. L_{DNA} and 3) determined the slope of the resulting curve by linear regression and counted the number of events with slope values $\geq 1.2352 - 0.052$ (as a measure for "false positives" in the context of our experiment). After a large number (50,000) of repetitions of 1)-3), the relative number of such events was found to be below $2 \cdot 10^{-5}$ (less than 1 event in 50,000, 3 repeats; mean of all simulated slopes: 1), cf. fig. S9. Thus, the probability that "true" scaling factor for this particular data set ($V_{bias} = -400$ mV) is actually 1.0 given the statistical basis, is negligibly small (and even smaller, taking into account all bias voltages).

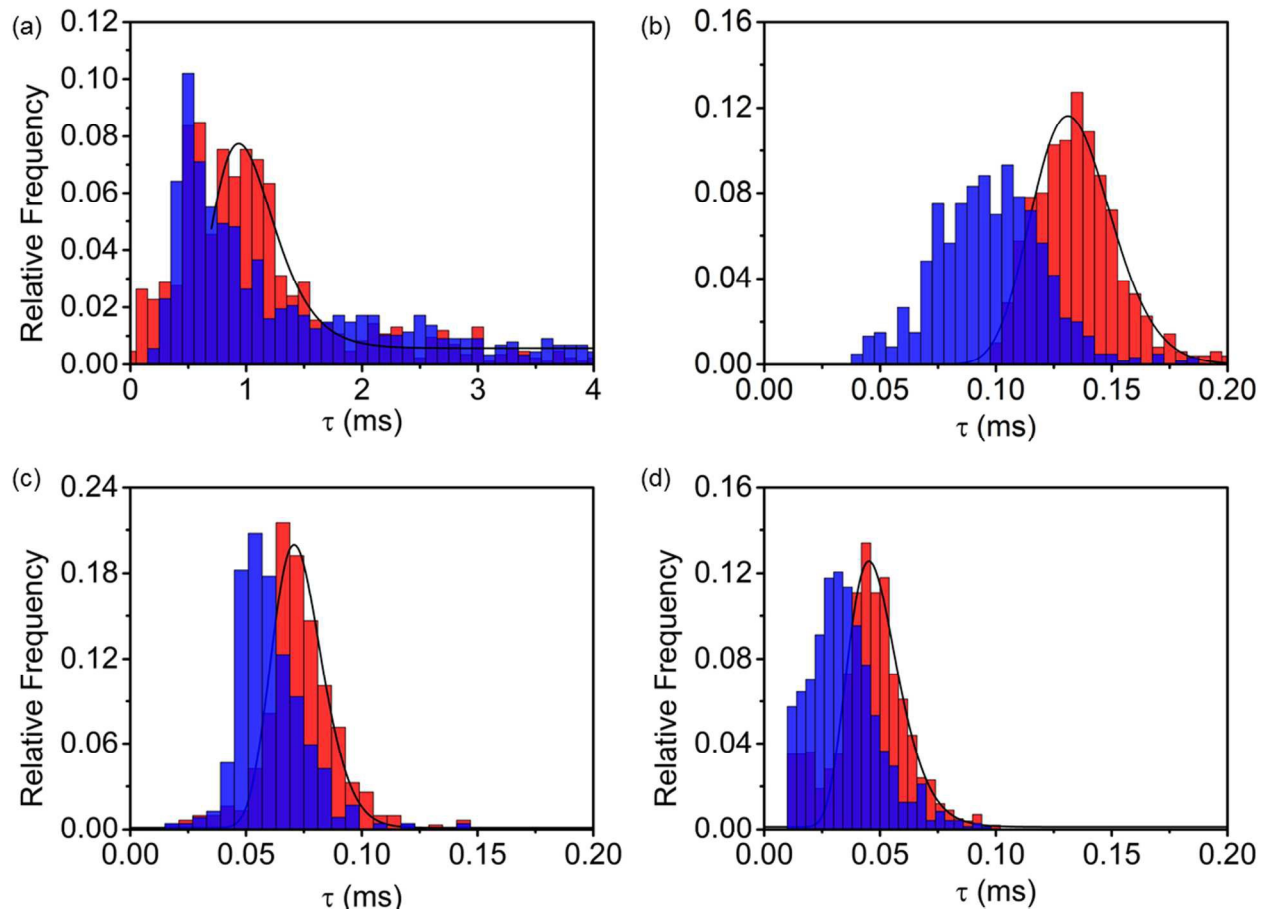


Figure 3. Typical τ histograms for (a) 48.5, (b) 10, (c) 5.31 and (d) 4 kbp dsDNA translocations with V_{bias} of -800 mV. The linear and folded population of events are shown in red and blue respectively. The linear population of events is fitted with a log-normal function and the most probable translocation time τ_{mp} extracted. At V_{bias} of -800 mV the $I(t)$ trace was filtered at 100 kHz for 48.5 kbp DNA and 200 kHz for 10, 5.31 and 4 kbp DNA.

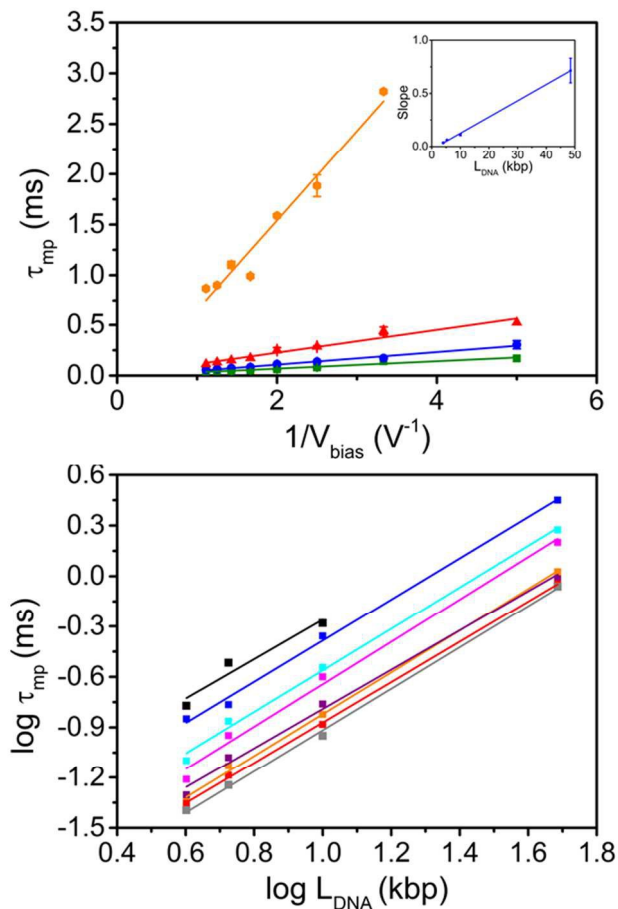


Figure 4. Translocation of linear DNA as a function of V_{bias}^{-1} and L_{DNA} . (a) Plot of τ_{imp} vs V_{bias}^{-1} for 48.5 (orange), 10 (red), 5.31 (blue) and 4 kbp (green) DNA. The slopes m were obtained as 0.715 ± 0.116 , 0.112 ± 0.009 , 0.062 ± 0.003 , 0.037 ± 0.003 for 48.5, 10, 5.31 and 4 kbp DNA, respectively. Inset: Plot of m vs. L_{DNA} , showing a linear dependence (slope = 0.0153 ± 0.0003 ; intercept = -0.027 ± 0.008 ; $R = 0.999$) (b) log-log plot of L_{DNA} versus τ_{imp} at V_{bias} -200 mV (black), -300 mV (blue), -400 mV (cyan), -500 mV (magenta), -600 mV (purple), -700 mV (orange), -800 mV (red) and -900 mV (grey). The scaling factor p is independent of V_{bias} within experimental error and equal to 1.22 ± 0.01 (average of all bias voltages measured).

In light of the variety of scaling factors reported in the literature and our own results, we then wondered whether surface adsorption of DNA could have an effect on the observed scaling factor.

Specifically, we extend the Ghosal model by including a friction term for the interaction between adsorbed DNA and the surface close to the pore (cf. Supporting Information for the derivation). In this model, DNA initially adsorbs to the membrane (or pipette) surface; one end of the DNA then enters the pore under the effect of the electric field and the strand is pulled through base pair by base pair. N_p and N_t are the total number of monomers (base pairs) in the DNA strand, and the number of monomers that have translocated at a given moment in time, respectively. The number of adsorbed monomers is equal to $N_{ads} = (N_p - N_t)^\alpha$, where α is an exponent that scales the number of monomers on the 'cis' side, $N_p - N_t$, to the number of monomers in contact with the surface. If $\alpha = 1$, then the DNA is fully relaxed and in a linear configuration, every monomer on the 'cis' side is in contact with the surface. If the DNA is still in a globular, non-equilibrated configuration, more akin to the state in solution, then $\alpha < 1$, depending on the exact shape. For simplicity, we will assume that α does not change during the translocation process. The friction force is given by:²⁴

$$F_R = N_{ads} \cdot \beta \cdot v = (N_p - N_t)^\alpha \cdot \beta \cdot v \quad (1)$$

where β and v are the friction coefficient and the translocation speed, respectively. v is a function of N_t , but we assume that for a given N_t , the sum of electrophoretic, viscous and friction force equal to zero:

$$F_e + F_v + F_R = 0 \quad (2)$$

The expressions for F_e and F_v can be found in the SI. Each monomer contributes a fraction of the translocation time $\Delta\tau = 1/v(N_t) \cdot d_N$, which when summed over all N_p gives the total translocation time τ :

$$\tau = \frac{\ln \frac{\alpha}{R} \cdot \beta \cdot d_N \cdot \sum_1^{N_p} (N_p - N_t)^\alpha}{2\pi\epsilon E_0 \cdot (\zeta_W - \zeta_p)} - \frac{\mu \cdot d_N \cdot N_p}{\epsilon E_0 \cdot (\zeta_W - \zeta_p)} \quad (3)$$

where a and R are the radius of the DNA and the (cylindrical) pore channel, d_N the distance between adjacent base pairs (0.34 nm/bp, so $L_{DNA} = N_p \cdot d_N$), ζ_w and ζ_p the zeta-potentials of the pore wall and the polymer, μ the dynamic viscosity, ϵ the dielectric constant ($\epsilon_r \epsilon_0$) and E_0 the electric field at the pore. Note that this expression ignores the effect of the membrane thickness on τ , which is a reasonable approximation for sufficiently long DNA (here $N_p > 10^3$). The summation can be solved analytically by Euler-Maclaurin summation or, for sufficiently large N_p , approximated by an integral. This gives

$$\sum_1^{N_p} (N_p - N_t)^\alpha \approx \frac{1}{\alpha+1} \cdot N_p^{\alpha+1} \quad (4)$$

and implies that $\log(\tau) \propto (\alpha+1) \cdot \log(N_p)$, i.e. $p = \alpha + 1$ between 1 and 2. In the opposite limit, when the friction term is negligible compared to the second term on the right-hand side of eq. (3), $\log(\tau) \propto \log(N_p)$ and $p = 1$ (note that $(\zeta_w - \zeta_p) < 0$ here). Figure 5 illustrates these two limits as well as intermediate values for experimentally determined β values ranging from very small to very large friction.²⁴

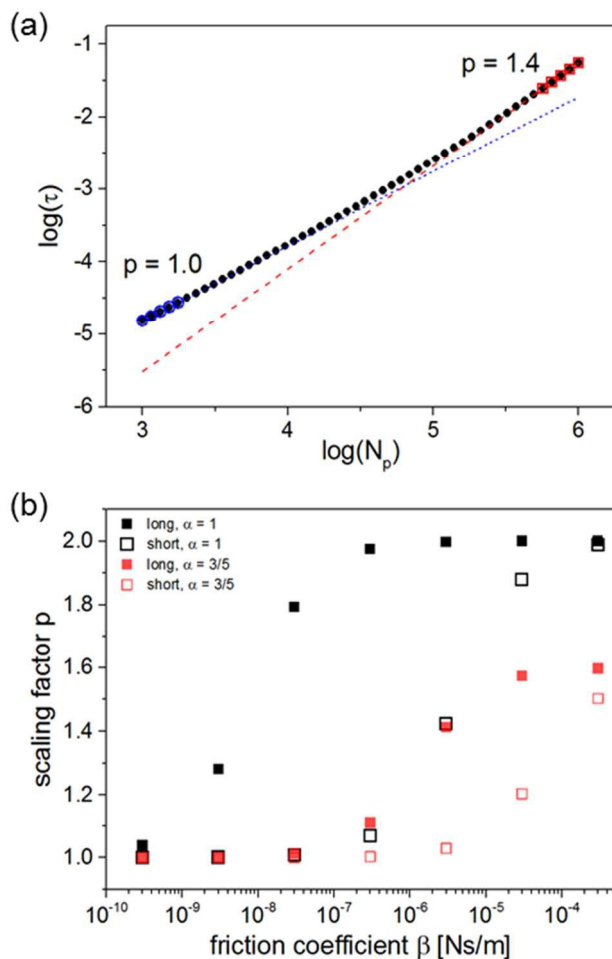


Figure 5. (a) Simulated $\log(\tau)$ vs. $\log(N_p)$ illustrating bi-phasic behavior for p , based on eq. (3), with $\beta = 3 \cdot 10^{-6}$ Ns/m (intermediate friction).²⁴ $p \rightarrow 1$ for short DNA (small N_p) in accordance with Ghosal's model; $p \rightarrow \alpha + 1$ for long DNA (large N_p , α here taken to be $3/5$ (Flory scaling)³⁵) (b) Scaling factor p as function of friction coefficient β , for two different values of α , and for short and long DNA, respectively (corresponding to the two limits of eq. (3), in terms of N_p).

This demonstrates that friction effects between DNA and the substrate surface can indeed result in values for p that are larger than 1 and similar in magnitude to previously observed experimental values, for realistic values of β . It does not rule out that the observed scaling behavior is a property

of the polymer itself (e.g. related to Flory scaling of the radius of gyration), but the present model does offer an explanation that reconciles differences in scaling factors observed with the same analyte (DNA), but with different platforms or experimental contexts. In fact, surface effects have been shown to have a significant impact on the translocation of proteins and protein/DNA complexes,^{36,37} and it is also well-known that the interaction between DNA and a surface is strongly dependent on the electrolyte composition.³⁸ To this end, the presence of Mg^{2+} results in the adsorption of DNA to mica, while preserving some strand mobility when bound to the surface (i.e. the DNA equilibrates after adsorbing). Other ions, such as Ni^{2+} or Mn^{2+} on the other hand cause strong adsorption and kinetic trapping of the DNA structure on the surface.

Careful experiments combining nanopore translocation and AFM pulling experiments, where the friction properties of the sensor surface are altered by chemical modification could be used to test the above hypothesis. These are non-trivial, however, and will have to be left for future work.

In conclusion, we have probed the translocation dynamics of four different lengths of dsDNA molecules through quartz nanopipettes using a custom-built high-speed electrical detection scheme. Our setup has allowed low-noise current measurements with a time resolution of up to $3.5 \mu s$ in 1 M KCl, demonstrating significantly improved high-speed and low-noise ionic current measurements in nanopipettes. Due to the low input capacitance of the custom CMOS current amplifier, a further increase in the filter frequency appears feasible by reducing the capacitance of the nanopipette and of the connecting wires. In contrast with previous reports using nanopipettes and LiCl electrolyte, we observe a scaling factor between DNA translocation time and length of $p = 1.22 \pm 0.01$, which is close to $p \approx 1.3$ observed in several translocation experiments with chip-based devices. The relatively wide range of observed scaling factors is difficult to reconcile with the conventional view

that the scaling factor results from hydrodynamic drag on the DNA globule at the pore entrance (i.e. the non-translocated section) and Flory scaling of the radius of gyration.¹⁴ It suggests that other effects, such as adsorption of the DNA to the membrane surface and resulting friction, may play a part in determining p , too. To investigate this effect, we derive an extension of Ghosal's model taking into account friction between DNA and the membrane surface outside of the pore (where the electric field is weak or negligible). This can lead to p values between 1 and 2, which approximately covers the range of experimentally observed values. Hence, DNA adsorption prior to translocation may be an important factor in translocation experiments, depending on the experimental conditions.

ASSOCIATED CONTENT

Supporting Information.

Gel electrophoresis confirming lengths and purity of DNA samples, comparison between Axopatch 200B and custom-built setup, comprehensive low-noise amplifier characterization, representative $I - V$ curves of nanopipettes used, typical scatter plots of τ vs. peak amplitude for the four L_{DNA} 's used, table of most probable τ values, a comparison between different fitting models for the DNA translocation time distribution, further details on the stochastic numerical simulation of the scaling statistics and the derivation of the extended model for the length dependence of τ .

AUTHOR INFORMATION

Corresponding Author

*Email: t.albrecht@imperial.ac.uk

Author Contributions

The manuscript was written through contributions of all authors. All authors have given approval to the final version of the manuscript. ‡These authors contributed equally. (match statement to author names with a symbol)

Funding Sources

RF would like to thank EPSRC for a PhD studentship.

Notes

ACKNOWLEDGMENT

REFERENCES

- (1) Bell, N. A. W.; Keyser, U. F. *J. Am. Chem. Soc.* **2015**, *137*, 2035–2041.
- (2) Li, W.; Bell, N. A. W.; Hernandez-Ainsa, S.; Thacker, V. V.; Thackray, A. M.; Bujdoso, R.; Keyser, U. F. *ACS Nano* **2013**, *7*, 4129–4134.
- (3) Steinbock, L. J.; Otto, O.; Chimere, C.; Gornall, J.; Keyser, U. F. *Nano Lett.* **2010**, *10*, 2493–2497.
- (4) Steinbock, L. J.; Steinbock, J. F.; Radenovic, A. *Nano Lett.* **2013**, *13*, 1717–1723.
- (5) Gibb, T. R.; Ivanov, A. P.; Edel, J. B.; Albrecht, T. *Anal. Chem.* **2014**, *86*, 1864–1871.
- (6) Gong, X.; Patil, A. V.; Ivanov, A. P.; Kong, Q.; Gibb, T.; Dogan, F.; deMello, A. J.; Edel, J. B. *Anal. Chem.* **2014**, *86*, 835–841.
- (7) Wang, Y.; Kececi, K.; Mirkin, M.; Mani, V. *Chem. Sci.* **2013**, *4*, 655–663.

- (8) Ivanov, A. P.; Actis, P.; Jo, P.; Edel, J. B.; Klenerman, D.; Korchev, Y. *ACS Nano* **2015**, *9*, 3587–3595.
- (9) Yu, J.; Lim, M.; Thi, D.; Huynh, N.; Kim, H.; Kim, H.; Kim, Y. *ACS Nano* **2015**, *9*, 5289–5298.
- (10) Steinbock, L. J.; Lucas, A.; Otto, O.; Keyser, U. F. *Electrophoresis* **2012**, *33*, 3480–3487.
- (11) Thacker, V. V.; Ghosal, S.; Hernandez-Ainsa, S.; Bell, N. A. W.; Keyser, U. F. *Appl. Phys. Lett.* **2012**, *101*, 223704.
- (12) Wanunu, M.; Morrison, W.; Rabin, Y.; Grosberg, A. Y.; Meller, A. *Nat. Nanotechnol.* **2010**, *5*, 160–165.
- (13) Li, J.; Talaga, D. S. *J. Phys. Condens. Matter* **2010**, *22*, 454129.
- (14) Storm, A. J.; Storm, C.; Chen, J.; Zandbergen, H.; Joanny, J. F.; Dekker, C. *Nano Lett.* **2005**, *5*, 1193–1197.
- (15) Lubensky, D. K.; Nelson, D. R. *Biophys. J.* **1999**, *77*, 1824–1838.
- (16) Reimann, P.; Meyer, A.; Getfert, S. *Biophys. J.* **2012**, *103*, 889–897.
- (17) Wanunu, M.; Sutin, J.; McNally, B.; Chow, A.; Meller, A. *Biophys. J.* **2008**, *95*, 4716–4725.
- (18) Doi, M.; Edwards, S. F. *The Theory of Polymer Dynamics*; Clarendon Press.
- (19) Bell, N. A. DNA Origami Nanopores and Single Molecule Transport through Nanocapillaries, Ph.D. Thesis, University of Cambridge, November 2013.
- (20) Ghosal, S. *Phys. Rev. Lett.* **2007**, *98*, 238104.
- (21) Ghosal, S. *Phys. Rev.* **2006**, *74*, 041901.
- (22) Uplinger, J.; Thomas, B.; Rollings, R.; Fologea, D.; McNabb, D.; Li, J. *Electrophoresis* **2012**, *33*, 3448–3457.

- (23) Ciccarella, P.; Carminati, M.; Ferrari, G.; Fraccari, R.; Bahrami, A. An Integrated Low-Noise Current Amplifier for Glass-Based Nanopore Sensing; 10th Conference on Ph.D. Research in Microelectronics and Electronics (PRIME 2014), Grenoble, France, June 29 - July 30, 2014, pp 1–4.
- (24) Kühner, F.; Erdmann, M.; Sonnenberg, L.; Serr, A.; Morfill, J.; Gaub, H. E. *Langmuir* **2006**, *22*, 11180–11186.
- (25) Ferrari, G.; Farina, M.; Guagliardo, F.; Carminati, M.; Sampietro, M. *Electron. Lett.* **2009**, *45*, 1278–1280.
- (26) Balan, A.; Machielse, B.; Niedzwiecki, D.; Lin, J.; Ong, P.; Engelke, R.; Shepard, K. L.; Drndic, M. *Nano Lett.* **2014**, *14*, 7215–7220.
- (27) Rosenstein, J. K.; Wanunu, M.; Merchant, C. A.; Drndic, M.; Shepard, K. L. *Nat. Methods* **2012**, *9*, 487–492.
- (28) Smeets, R. M. M.; Keyser, U. F.; Krapf, D.; Wu, M.; Dekker, N. H.; Dekker, C. *Nano Lett.* **2006**.
- (29) Ling, D. Y.; Ling, X. S. *J. Phys. Condens. Matter* **2013**, *25*, 375102.
- (30) Wu, H.; Liu, H.; Tan, S.; Yu, J.; Zhao, W.; Wang, L.; Liu, Q. *J. Phys. Chem. C* **2014**, *118*, 26825–26835.
- (31) Fologea, D.; Brandin, E.; Uplinger, J.; Branton, D.; Li, J. *Electrophoresis* **2007**, *28*, 3186–3192.
- (32) Kowalczyk, S. W.; Hall, A. R.; Dekker, C. *Nano Lett.* **2010**, *10*, 324–328.
- (33) Kowalczyk, S. W.; Wells, D. B.; Aksimentiev, A.; Dekker, C. *Nano Lett.* **2012**, *12*, 1038–1044.
- (34) Clauset, A.; Shalizi, C. R.; Newman, M. E. J. *SIAM Rev.* **2009**, *51*, 661.

- (35) Israelachvili, J. N., *Intermolecular and Surface Forces*, 3rd edition; Academic press, **2011**, pp 382.
- (36) Japrun, D.; Bahrami, A.; Nadzeyka, A.; Peto, L.; Bauerdick, S.; Edel, J.B.; Albrecht, T. *J. Phys. Chem. B* **2014**, 118, 11605-11612.
- (37) Nuttall, P.; Lee, K.; Ciccarella, P.; Carminati, M.; Ferrari, G.; Kim, K.-B.; Albrecht, T. *J. Phys. Chem. B* **2016**, DOI: 10.1021/acs.jpcc.5b11076.
- (38) Rivetti C.; Guthold, M.; Bustamante C. *J. Mol. Biol.* **1996**, 264, 919-932.

TOC image

